

ARTICLE

Received 28 Dec 2015 | Accepted 28 Apr 2016 | Published 3 Jun 2016

DOI: 10.1038/ncomms11796

OPEN

# Interface strain in vertically stacked two-dimensional heterostructured carbon-MoS<sub>2</sub> nanosheets controls electrochemical reactivity

Landon Oakes<sup>1,2</sup>, Rachel Carter<sup>1</sup>, Trevor Hanken<sup>1</sup>, Adam P. Cohn<sup>1</sup>, Keith Share<sup>1,2</sup>, Benjamin Schmidt<sup>3</sup> & Cary L. Pint<sup>1,2,3</sup>

Two-dimensional (2D) materials offer numerous advantages for electrochemical energy storage and conversion due to fast charge transfer kinetics, highly accessible surface area, and tunable electronic and optical properties. Stacking of 2D materials generates heterogeneous interfaces that can modify native chemical and physical material properties. Here, we demonstrate that local strain at a carbon-MoS<sub>2</sub> interface in a vertically stacked 2D material directs the pathway for chemical storage in MoS<sub>2</sub> on lithium metal insertion. With average measured MoS<sub>2</sub> strain of ~0.1% due to lattice mismatch between the carbon and MoS<sub>2</sub> layers, lithium insertion is facilitated by an energy-efficient cation-exchange transformation. This is compared with low-voltage lithium intercalation for unstrained MoS<sub>2</sub>. This observation implies that mechanical properties of interfaces in heterogeneous 2D materials can be leveraged to direct energetics of chemical processes relevant to a wide range of applications such as electrochemical energy storage and conversion, catalysis and sensing.

<sup>1</sup>Department of Mechanical Engineering, Vanderbilt University, Nashville, Tennessee 37235, USA. <sup>2</sup>Interdisciplinary Materials Science Program, Vanderbilt University, Nashville, Tennessee 37235, USA. <sup>3</sup>Vanderbilt Institute of Nanoscale Science and Engineering, Vanderbilt University, Nashville, Tennessee 37235, USA. Correspondence and requests for materials should be addressed to C.L.P. (email: cary.l.pint@vanderbilt.edu).

**2D** graphene and transition metal dichalcogenide (TMDC) materials have captivated researchers in the past decade owing to a set of unique physical and chemical properties that deviate from their bulk analogues and the exploitation of these properties in broad applications<sup>1</sup>. Specifically for electronics, vertical integration of 2D materials enables logic component design with high on-off ratio and promise for three-dimensional (3D) electronics that progress beyond silicon<sup>2–8</sup>. In semiconductor electronics, engineering 2D TMDC materials using strain applied at an interface has been shown to strongly modulate the bandgap and band structure, which results in modified electrical and optical properties for strained materials<sup>9–14</sup>. For monolayer MoS<sub>2</sub>, the bandgap is observed to shift by up to 15 meV under tensile strain of up to 4.8% (ref. 15), and for multilayered WSe<sub>2</sub> the bandgap transitions from indirect to direct under strain of up to 2% (ref. 16). Theoretical efforts have further emphasized strain-enabled broadband absorption and photodetection in MoS<sub>2</sub>, even though this has not yet been experimentally realized<sup>17</sup>. The intersection of strain-engineered properties of 2D materials and heterostructured vertically integrated interfaces of 2D materials presents an engaging research area for next-generation electronics. Nonetheless, such materials and research directions remain elusive for many other applications of 2D materials.

On this front, 2D materials and specifically 2D TMDCs have demonstrated excellent performance in a range of electrochemical applications including lithium- and sodium-ion batteries<sup>18–20</sup>, photocatalytic conversion<sup>21–23</sup> and biosensing applications<sup>24–26</sup>. Unlike electronic devices, these applications require bulk-like quantities of 2D materials—a challenge aided by recent developments in the liquid exfoliation and assembly of layered TMDCs<sup>27–29</sup>. However, addressing how properties in heterostructured or complex 2D materials can impact chemical processes responsible for electrochemical applications is hampered by uniform material fabrication routes that can be used on scales required for electrochemical measurements. As a result, the impact of strained interfaces in 2D materials on chemical and electrochemical processes remains virtually unstudied. Only recently has an observation emerged that compressive strain on Pt catalysts can improve the oxygen reduction reaction capability of Pt relevant to fuel cells<sup>30</sup>. In this manner, 2D materials provide an ideal test bed for the understanding of how interfaces and strain can impact electrochemical processes, motivated by pioneering efforts in the field of semiconductor electronics.

This is the focus of this report, which documents that interface strain measured over statistical quantities of stacked 2D carbon-MoS<sub>2</sub> heterostructured nanosheets can be directly correlated with distinct differences in chemical processes occurring in 2D materials. In particular, combining optical and electrochemical techniques we demonstrate that strain engineering of interfaces can enable control of the energetic pathway for the chemical conversion of MoS<sub>2</sub> into electrochemically active Mo and Li<sub>2</sub>S<sub>n</sub> species during reaction with lithium. This highlights the important role that mechanical strain can have in engineering energy storage processes in materials.

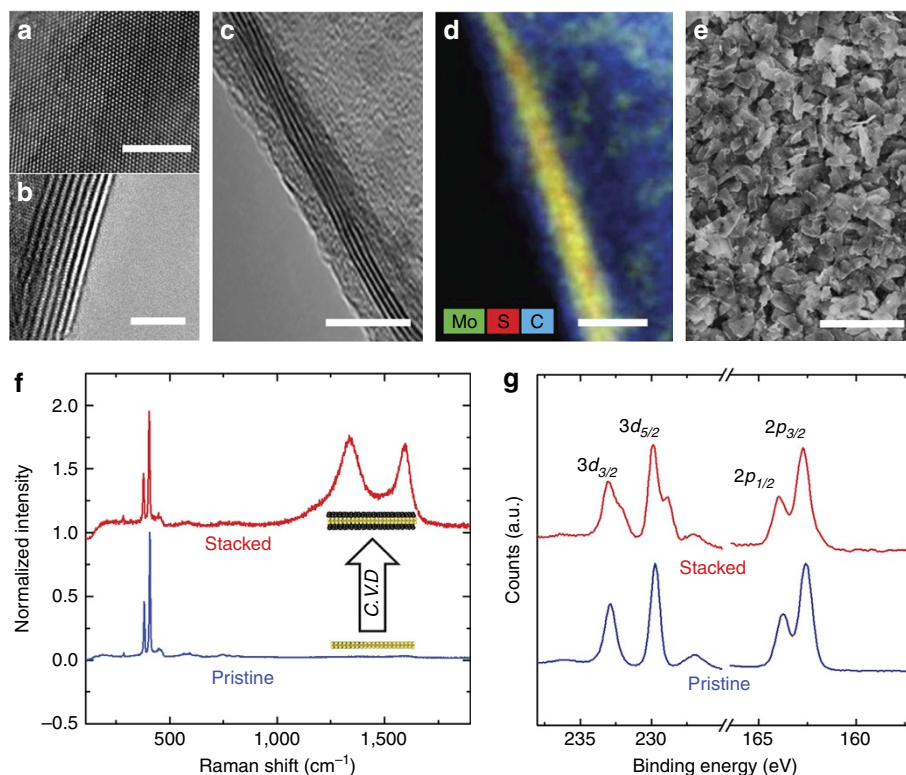
## Results

**Fabrication of interface-strained materials.** MoS<sub>2</sub> nanosheets were produced through liquid exfoliation of bulk MoS<sub>2</sub> powders in *n*-methyl-2-pyrrolidone (NMP) solvents and subsequent centrifugation. Transmission electron microscopy (TEM) of a representative exfoliated MoS<sub>2</sub> nanosheet is shown in Fig. 1a,b. Interlayer spacing of ~0.61 nm is observed for MoS<sub>2</sub> nanosheets, with thicknesses ranging from 2–15 atomic layers (Supplementary Fig. 1, Supplementary Note 1). Ultrathin carbon

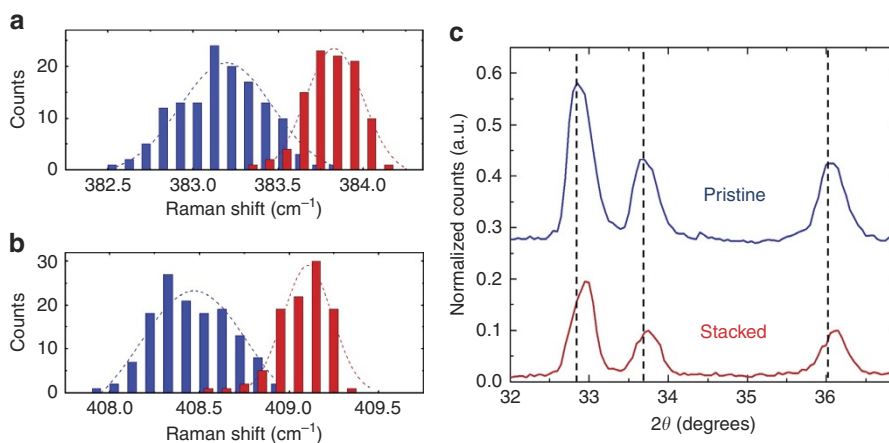
layers are grown directly on the MoS<sub>2</sub> surface through MoS<sub>2</sub> catalysed decomposition of C<sub>2</sub>H<sub>2</sub> precursors using a temperature ramp chemical vapour deposition process (Supplementary Fig. 2) that is capable of gram-scale batch processing. This generates vertically stacked architectures where ultrathin carbon layers are formed on both sides of the MoS<sub>2</sub> nanosheets, with a representative TEM image of this architecture shown in Fig. 1c, and corresponding elemental analysis map in Fig. 1d. To produce an appreciable mass of material for electrochemical tests, electrophoretic deposition was used to assemble the vertically stacked carbon-interfaced MoS<sub>2</sub> (C-MoS<sub>2</sub>) nanosheets into conformal films on metal substrates from NMP dispersions following chemical vapour deposition (Fig. 1e; Supplementary Fig. 3, Supplementary Note 2). All aspects of synthesis and processing of C-MoS<sub>2</sub> materials are chosen to be compatible with scalable processing, and ongoing research efforts to improve the simplicity and scalability of liquid exfoliation can further improve this<sup>31</sup>. Raman spectroscopy analysis (Fig. 1f) of vertically stacked C-MoS<sub>2</sub> nanosheets indicates that vertical stacks maintain an identical signature of crystalline MoS<sub>2</sub> following the carbon synthesis based on  $E_{2g}$  and  $A_{1g}$  modes (300–500 cm<sup>-1</sup>). The carbon layers exhibit a significant amount of  $sp^3$  hybridized carbon atoms (~1,320 cm<sup>-1</sup>, or D-band) relative to  $sp^2$  carbon species (~1,580 cm<sup>-1</sup>, or G-band). Whereas this indicates the presence of carbon, X-ray photoelectron spectroscopy (XPS) indicates the emergence of both a peak in the sulfur  $2p_{3/2}$  and  $2p_{5/2}$  spectra at low-binding energies, as well as shoulders in both Mo  $3d_{5/2}$  and  $3d_{3/2}$  peaks that represent a modulation to the local bonding environment in the crystal (Fig. 1g). Notably, the existence of the low-energy shoulder in the sulfur  $2p$  and Mo  $3d$  peaks is consistent with the formation of the metallic 1T-phase of MoS<sub>2</sub> produced from the strain-induced distortion of sulfur atoms observed previously (Supplementary Fig. 4, Supplementary Note 3)<sup>32</sup>. This analysis collectively supports the formation of a distinct carbon-MoS<sub>2</sub> stacked interface, where mismatch of the in-plane lattice spacing between MoS<sub>2</sub> and carbon will induce significant interface strain that propagates into the MoS<sub>2</sub> nanosheet from the C-MoS<sub>2</sub> interface.

To assess strain in the vertically stacked 2D material, statistical Raman spectroscopy mapping comprising over 200 individual scans in separate areas was performed on the  $E_{2g}$  and  $A_{1g}$  modes of MoS<sub>2</sub>, which are highly sensitive to tensile or compressive strain<sup>33–35</sup>. (Fig. 2a,b) On the basis of the peak-to-peak analysis of Raman mode distributions, blue-shifts of ~0.66 cm<sup>-1</sup> and ~0.59 cm<sup>-1</sup> were observed for the  $E_{2g}$  and  $A_{1g}$  modes, respectively. Asymmetry in these modes is expected and attributed to stronger electronic coupling to the  $A_{1g}$  mode<sup>36</sup>. This yields an ~0.1–0.2% compressive strain based on relative  $A_{1g}$  mode shifts in accordance with previous studies<sup>9,34</sup>, supporting the presence of interface-induced compressive strain on the MoS<sub>2</sub> material. This is further confirmed using X-ray diffraction which demonstrates a similar ~0.1% compressive strain due to vertical stacking based on analysis of the (100) and (110) low-index planes of MoS<sub>2</sub> (Fig. 2c). We anticipate this measured strain to be present at both the interface and on the interior of the nanosheets as they possess a thickness well below the critical layer thickness at which strain relaxation occurs<sup>37</sup>.

**Controlling electrochemical processes using strain.** To assess how the vertically stacked architecture and interface strain influences electrochemical processes, we combined electrophoretically assembled vertically stacked 2D C-MoS<sub>2</sub> nanosheets with Li metal electrodes, and a 1.0M lithium hexafluorophosphate solution in ethylene carbonate and diethyl carbonate electrolyte, and compared the electrochemical



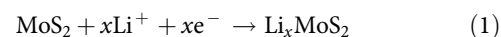
**Figure 1 | Synthesis of vertically stacked carbon-MoS<sub>2</sub> heterostructured nanosheets.** (a,b) TEM images of pristine exfoliated MoS<sub>2</sub> nanosheets. (c) Edge-view TEM image of a vertically stacked carbon-MoS<sub>2</sub> (C-MoS<sub>2</sub>) nanosheet. (d) Energy-dispersive X-ray spectroscopy analysis of a stacked C-MoS<sub>2</sub> nanosheet. The coloured inset describes the colour assignment of each mapped element, overlapping Mo and S signals appear yellow in the image. (e) Scanning electron microscopy image of an electrophoretically assembled electrode material formed with stacked C-MoS<sub>2</sub> nanosheets. Scale bars, 4 nm (a,b) 10 nm (c,d) and 1 μm (e). (f) Raman spectroscopy and (g) X-ray photoelectron spectroscopy of pristine MoS<sub>2</sub> nanosheets and stacked C-MoS<sub>2</sub> nanosheets.



**Figure 2 | Interface strain in vertically stacked 2D C-MoS<sub>2</sub> nanosheets.** Distributions from Raman spectroscopy maps comprising >100 individual scans showing average shifts in the MoS<sub>2</sub> (a) E<sub>2g</sub> and (b) A<sub>1g</sub> modes due to strain induced by a lattice mismatched carbon-MoS<sub>2</sub> interface. The dotted lines overlaying each distribution represent Gaussian fits to the distribution data. (c) X-ray diffraction analysis of vertically stacked C-MoS<sub>2</sub> nanosheets indicating stacking-induced strain in low-index planes. The following planes can be assigned to the X-ray diffraction spectra:  $2\theta = 32.6^\circ$  is (100),  $2\theta = 33.5^\circ$  is (101) and  $2\theta = 35.8^\circ$  is (102). The vertical dotted lines emphasize the difference in peak positions between the two spectra.

properties against similar electrode materials produced with pristine MoS<sub>2</sub> nanosheets (Supplementary Figs 5,6, Supplementary Notes 4,5). Cyclic voltammetry scans of these electrodes and corresponding differential capacity plots based on galvanostatic measurements are shown in Fig. 3. As these two electrode materials differ only by the presence of a vertically stacked C-MoS<sub>2</sub> interface, electrochemical data indicates significant changes to the chemical processes occurring on

lithium insertion into the MoS<sub>2</sub> material. For pristine MoS<sub>2</sub> nanosheets, two subsequent reactions are observed, with the first one at ~1.1 V and the second at ~0.55 V versus Li/Li<sup>+</sup>. (Fig. 3a,b) This is consistent with the known pathways for insertion of lithium into pristine MoS<sub>2</sub>, which occurs first through an intercalation reaction (1.1 V) that follows



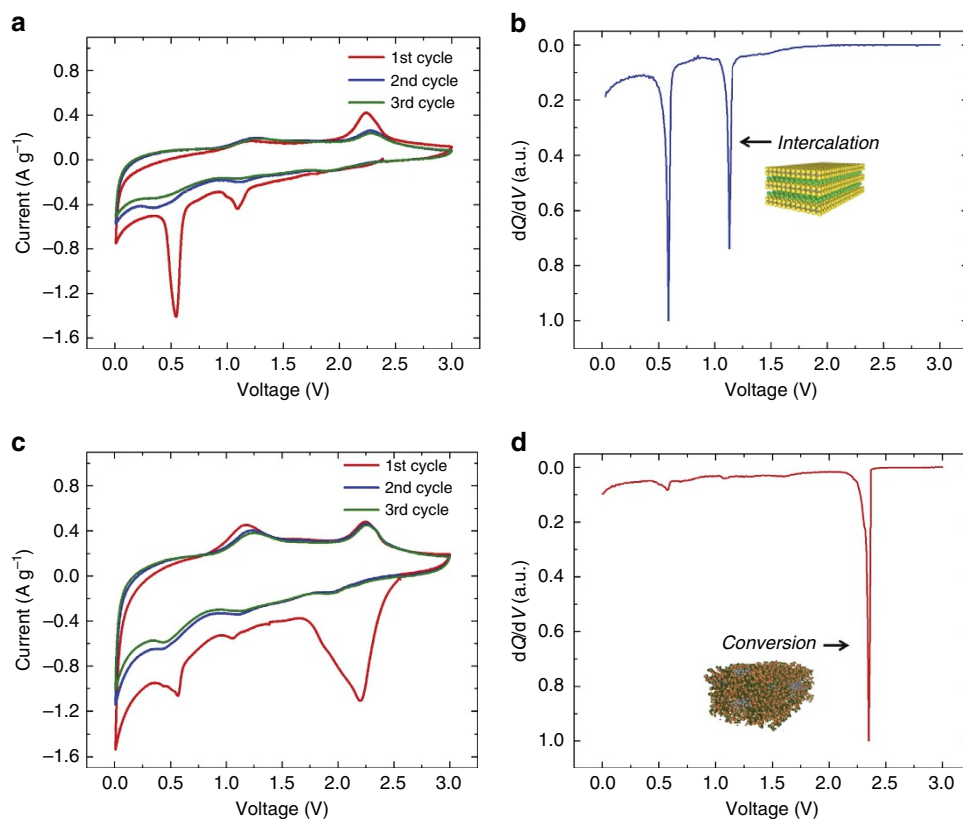
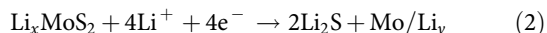


**Figure 3 | Electrochemical assessment of strained carbon-MoS<sub>2</sub> heterostructured nanosheets.** (a) CV and (b) normalized differential capacity measurements for MoS<sub>2</sub> under lithium insertion and extraction, with an arrow indicating the potential of the intercalation reaction that occurs in pristine MoS<sub>2</sub> materials. (c) CV and (d) normalized differential capacity plots for vertically stacked C-MoS<sub>2</sub> nanosheets, with an arrow indicating the electrochemical signature of direct chemical conversion.

where MoS<sub>2</sub> undergoes a transition from a semiconducting 2H phase to the metallic 1T phase due to strain-induced deformation of the crystal from lithium ion insertion. Following this transition, the MoS<sub>2</sub> can undergo a subsequent conversion reaction at lower voltages (0.55 V) that follows



In contrast to this, insertion of lithium into the vertically stacked C-MoS<sub>2</sub> nanosheets yields a chemical reaction evident at ~2.3 V versus Li/Li<sup>+</sup> based on both CV and differential capacity curves (Fig. 3c,d) which is close to the open-circuit voltage (OCV) of the device. This reaction proceeds in the absence of Li intercalation into MoS<sub>2</sub> and no significant signature of lithium insertion at lower voltages occurs such as in pristine MoS<sub>2</sub> nanosheet electrodes. This highlights the presence of a chemical storage process occurring in vertically stacked C-MoS<sub>2</sub> materials that is not observed in pristine MoS<sub>2</sub> materials (Fig. 4a) and that interface-induced strain can directly trigger chemical conversion at practical voltages. It is important to note that these results distinguish the stacked C-MoS<sub>2</sub> configuration from simple mixtures of carbon nanomaterials and MoS<sub>2</sub> nanosheets which have been reported previously<sup>38–42</sup>, in two key ways, namely that the grown carbon layer induces interface strain not possible in weakly adhered mechanically mixed materials that modulates the chemical reactivity of the MoS<sub>2</sub> nanosheet toward chemical conversion, and that the stacked configuration provides a physical barrier to inhibit polysulfide dissolution into the electrolyte in a manner consistent with a yolk-shell confinement strategy<sup>43</sup>. However, the benefits reported in other studies by combining MoS<sub>2</sub> and carbons through mixing are also maintained in our study as evidenced by galvanostatic studies indicating better rate

capability and improved storage capacity at high rates for the C-MoS<sub>2</sub> electrodes (Supplementary Fig. 7). In addition, whereas the correlation between X-ray diffraction, Raman spectroscopy and XPS indicate the presence of strain due to the mismatch of in-plane lattice parameters of the stacked materials below the critical thickness, charge transfer effects between the C and MoS<sub>2</sub> materials can play a role in the origin of strain measured using these techniques. We also observe the lack of any electrochemical signature of lithium intercalation into the ultrathin carbon coating, implying that stacked C-MoS<sub>2</sub> nanosheets exhibit differences from pristine nanosheets that can be explained by compressive strain imposed on the 2D MoS<sub>2</sub> material.

To address the effect of the C-MoS<sub>2</sub> interface on the electrochemical properties during lithium insertion, Raman spectroscopy of the electrophoretically assembled MoS<sub>2</sub>-based electrodes at different cathodic potentials was carried out (Fig. 4b). This analysis is possible due to the preparation of electrodes in a manner that does not require binder materials often used in conventional battery electrodes that can overwhelm the desired Raman spectroscopic features. At OCV conditions, both electrode materials exhibit only the native Raman modes of MoS<sub>2</sub>. Cathodic scans from OCV conditions to 1.75 V versus Li/Li<sup>+</sup>—an energy below the Li<sup>+</sup> insertion reaction observed for vertically stacked C-MoS<sub>2</sub> nanosheets, yields no change for the pristine MoS<sub>2</sub> nanosheets, but the emergence of a distinct Raman peak at 746 cm<sup>-1</sup> is observed for the stacked C-MoS<sub>2</sub> nanosheets. This mode is due to the formation of lithium polysulfides (Li<sub>2</sub>S<sub>*n*</sub>, for 4 ≤ *n* ≤ 8) that can be attributed to chemical conversion of the MoS<sub>2</sub> into reaction products in a manner consistent with equation (2) (ref. 44). Correspondingly, a decrease of the MoS<sub>2</sub>

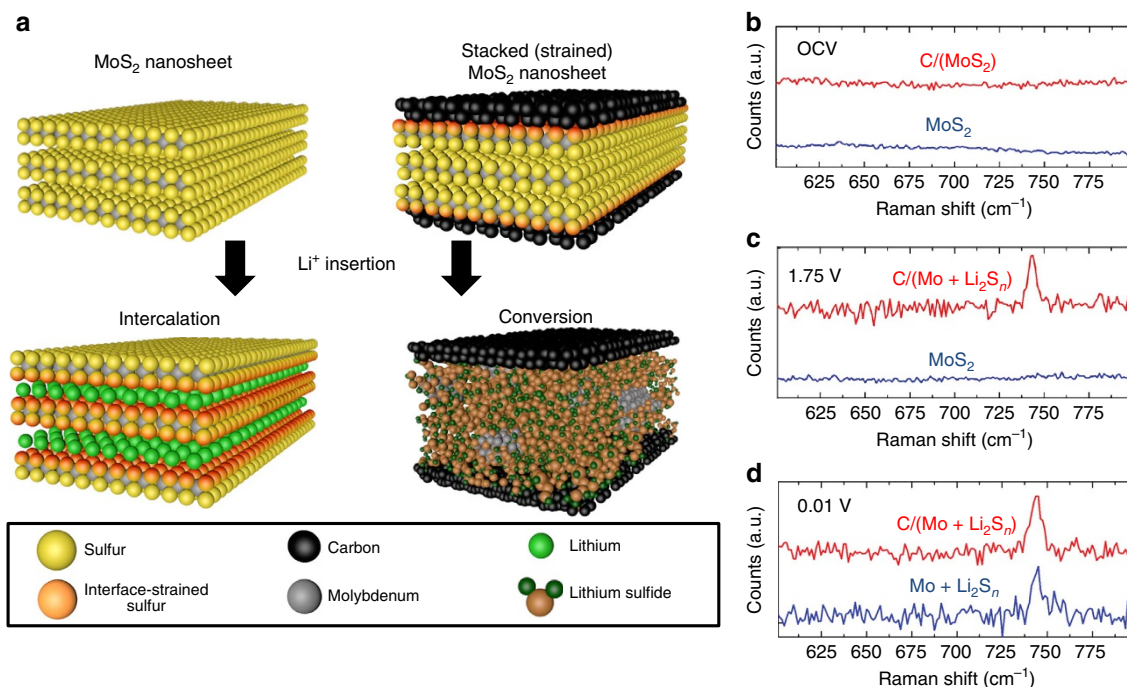


**Figure 4 | Strain-induced modulation of chemical conversion in vertically stacked C-MoS<sub>2</sub> nanosheets.** (a) Scheme showing the different chemical states between interface-strained MoS<sub>2</sub> nanosheets and pristine MoS<sub>2</sub> nanosheets after Li insertion, showing chemical conversion for stacked C-MoS<sub>2</sub> and intercalation for pristine MoS<sub>2</sub>. *Ex situ* Raman spectroscopy confirming the electrochemical signature of chemical conversion based on the Raman mode of polysulfides at 746 cm<sup>-1</sup> is presented for both materials at (b). Open-circuit voltage (OCV), (c) 1.75 V and (d) 0.01 V versus Li/Li<sup>+</sup>. Notably, at 1.75 V versus Li/Li<sup>+</sup>, the vertically stacked C-MoS<sub>2</sub> nanosheets have undergone chemical conversion, whereas the pristine MoS<sub>2</sub> nanosheets remain unconverted.

$A_{1g}$  and  $E_{2g}$  modes are observed as expected from conversion (Supplementary Fig. 8, Supplementary Note 6). This confirms that the high voltage  $\sim 2.3$  V signature in the CV and differential capacity curves for vertically stacked C-MoS<sub>2</sub> nanosheets (Fig. 3c,d) is a chemical conversion process similar to that which is known to occur at low voltages (0.55 V) in pristine MoS<sub>2</sub>. To further support this, cathodic scans were continued down to 0.01 V versus Li/Li<sup>+</sup> for the pristine MoS<sub>2</sub> electrode, where the signature of conversion is evident due to the presence of the Raman mode at 746 cm<sup>-1</sup>. Despite the difference in voltage of the conversion reactions between MoS<sub>2</sub> and C-MoS<sub>2</sub>, similar Raman spectroscopic signatures of the polysulfide conversion product and similar post-conversion redox energetics in both cases implies that the resulting chemical state of the material in both conversion reactions is the same. To further support this, we performed *in situ* electrochemical impedance spectroscopy (EIS, Supplementary Fig. 9, Supplementary Table 1), where EIS analysis was performed at the same voltages as those assessed using Raman spectroscopy. EIS studies elucidate a picture consistent with Raman spectroscopy results that indicates the electrochemical signature of conversion in different voltage regimes for the pristine MoS<sub>2</sub> and the stacked C-MoS<sub>2</sub>, respectively (Supplementary Note 7).

## Discussion

On the basis of the combined spectroscopic and electrochemical analysis, a picture emerges emphasizing the role of interface strain on lithium insertion in vertically stacked C-MoS<sub>2</sub> materials. In the pristine semiconducting 2H phase of MoS<sub>2</sub>, conversion of MoS<sub>2</sub> nanosheets cannot occur at voltages above where intercalation occurs (1.1 V versus Li/Li<sup>+</sup>) and can only proceed in a two-step chemical process following an intercalation reaction. As many researchers have discussed the promise of MoS<sub>2</sub> nanosheets for battery cathodes, the requirement of a

conversion reaction that is near the reduction potential of lithium is highly impractical in full-cell architectures. In a vertically stacked C-MoS<sub>2</sub> nanosheet, the interface strain due to lattice mismatch in a carbon-MoS<sub>2</sub> solid–solid interface leads to an average  $\sim 0.1\%$  compressive strain that propagates into the MoS<sub>2</sub> nanosheet lattice and enables control of the energetics of chemical conversion. In this regard, interface strain provides the appropriate energetic landscape to sustain direct conversion at voltages that enable pairing with conventional anode materials such as silicon or graphite which give promise to practical incorporation of this device in a full-cell battery configuration. This distinctive difference in the chemical pathways achieved during lithium insertion as a result of interface strain is illustrated in Fig. 4a, where the chemical state of the 2D materials is drastically different following a cathodic scan to 1 V.

The broader use of controlled interface mechanics to modify chemical pathways in low-dimensional materials presents an unexplored horizon for engineered low-dimensional nanostructures. This utilizes 2D materials as a framework to merge concepts of strain engineering with mechanochemistry to control the energetics of chemical processes relevant to energy storage, energy conversion, catalysis, and sensing applications. Building from our results showing that strained interfaces in vertically stacked C-MoS<sub>2</sub> nanosheets can modulate electrochemical reactivity, we envision a new paradigm for material design that exploits interface strain and mechanics as a versatile toolbox to modulate performance of designer 2D materials in diverse applications.

## Methods

**MoS<sub>2</sub> nanosheet synthesis.** In all, 500 mg of bulk MoS<sub>2</sub> powder (Aldrich, particle size  $< 2 \mu\text{m}$ ) was added to 50 ml of 1-methyl-2-pyrrolidinone (Aldrich, 99.5% anhydrous). The solution was sonicated in a bath sonicator for 12 h using  $8 \times 90$  min intervals. After sonication, the solution was centrifuged at 2,000 r.p.m. for 40 min. The upper 2/3 of the supernatant was removed and subsequently

centrifuged for 1 h at 5,000 r.p.m. before the excess supernatant was removed and the accumulated nanosheets were placed under vacuum overnight to completely evaporate the solvent.

**Vertically stacked carbon-MoS<sub>2</sub> nanosheet synthesis.** MoS<sub>2</sub> nanosheets contained within an alumina boat were placed into a 1-inch tube furnace and the tube was evacuated to 2 mTorr. A gas mixture of 100 standard cubic centimeters per minute (sccm) Ar and 20 sccm H<sub>2</sub> maintained at atmospheric pressure were introduced during ramping to a temperature 750 °C. At 750 °C, 2 sccm of acetylene (C<sub>2</sub>H<sub>2</sub>) was introduced for 10 min followed by a temperature ramp to 850 °C and an additional 10 min soak, and a final ramp to 950 °C for 10 min. After this process, the acetylene was turned off and the furnace cooled back down under a flow of argon and hydrogen, where materials were removed.

**Electrophoretic deposition.** A total of 20 mg of vertically stacked C-MoS<sub>2</sub> or pristine MoS<sub>2</sub> nanosheets were suspended in 20 ml NMP and sonicated for 30 min. Following this, a stainless steel spacer was placed at 0.5 cm from a 1 × 1 cm stainless steel counter electrode. A voltage of 30 V was applied for 30 min before carefully removing the coated steel electrode from solution and placing this into a vacuum chamber overnight to dry the sample.

**Electrochemical device fabrication and testing.** Electrochemical half-cell devices were assembled in an argon glovebox using CR 2,032 stainless steel coin cells purchased from MTI. The coated steel discs were separated from a lithium metal anode by a 2,500 Celgard separator saturated with a 1 M LiPF<sub>6</sub> in 1 g per 1 ml solution of ethylene carbonate and diethyl carbonate. Cyclic voltammetry scans and galvanostatic measurements were performed using a Metrohm autolab multichannel testing system.

**Material characterization.** Raman measurements were performed using a Renishaw inVia confocal Raman spectrometer. Micro-Raman maps were collected using a 532 nm laser. Before characterizing the electrodes after electrochemical testing, coin cells were disassembled in an Ar filled glovebox and the electrodes washed with an EC/DEC solution. TEM analysis was performed by drop casting a solution of pristine or stacked MoS<sub>2</sub> materials onto amorphous carbon TEM grids and then imaged using an FEI Osiris TEM at a beam voltage of 200 kV. X-ray diffraction was performed on powder samples using a Scintag XGEN 4,000 system with a CuK $\alpha$  (wavelength = 0.154 nm) radiation source. XPS was collected using a PHI 5,000 Versaprobe. Measurements were collected at a 45° takeoff angle with a 100  $\mu$ m spot size with charge neutralization.

**Data availability.** The data that support the findings of this study are available from the corresponding author upon request.

## References

- Liu, J. H. & Liu, X. W. Two-dimensional nanoarchitectures for lithium storage. *Adv. Mater.* **24**, 4097–4111 (2012).
- Gong, Y. J. *et al.* Vertical and in-plane heterostructures from WS<sub>2</sub>/MoS<sub>2</sub> monolayers. *Nat. Mater.* **13**, 1135–1142 (2014).
- Wang, X. & Xia, F. Van der Waals heterostructures: stacked 2D materials shed light. *Nat. Mater.* **14**, 264–265 (2015).
- Yu, W. J. *et al.* Vertically stacked multi-heterostructures of layered materials for logic transistors and complementary inverters. *Nat. Mater.* **12**, 246–252 (2013).
- Jariwala, D., Sangwan, V. K., Lauhon, L. J., Marks, T. J. & Hersam, M. C. Emerging device applications for semiconducting two-dimensional transition metal dichalcogenides. *ACS Nano* **8**, 1102–1120 (2014).
- Britnell, L. *et al.* Strong light-matter interactions in heterostructures of atomically thin films. *Science* **340**, 1311–1314 (2013).
- Hong, X. *et al.* Ultrafast charge transfer in atomically thin MoS<sub>2</sub>/WS<sub>2</sub> heterostructures. *Nat. Nanotechnol.* **9**, 682–686 (2014).
- Lee, G.-H. *et al.* Flexible and transparent MoS<sub>2</sub> field-effect transistors on hexagonal boron nitride-graphene heterostructures. *ACS Nano* **7**, 7931–7936 (2013).
- Li, M.-Y. *et al.* Epitaxial growth of a monolayer WSe<sub>2</sub>-MoS<sub>2</sub> lateral pn junction with an atomically sharp interface. *Science* **349**, 524–528 (2015).
- Georgiou, T. *et al.* Vertical field-effect transistor based on graphene-WS<sub>2</sub> heterostructures for flexible and transparent electronics. *Nat. Nanotechnol.* **8**, 100–103 (2013).
- He, J. *et al.* Electron transfer and coupling in graphene-tungsten disulfide van der Waals heterostructures. *Nat. Commun.* **5**, 5622 (2014).
- Roy, K. *et al.* Graphene-MoS<sub>2</sub> hybrid structures for multifunctional photoresponsive memory devices. *Nat. Nanotechnol.* **8**, 826–830 (2013).
- Castellanos-Gomez, A. *et al.* Local strain engineering in atomically thin MoS<sub>2</sub>. *Nano Lett.* **13**, 5361–5366 (2013).
- He, K., Poole, C., Mak, K. F. & Shan, J. Experimental demonstration of continuous electronic structure tuning via strain in atomically thin MoS<sub>2</sub>. *Nano Lett.* **13**, 2931–2936 (2013).
- Liu, Z. *et al.* Strain and structure heterogeneity in MoS<sub>2</sub> atomic layers grown by chemical vapour deposition. *Nat. Commun.* **5**, 5246 (2014).
- Desai, S. B. *et al.* Strain-induced indirect to direct bandgap transition in multi layer WSe<sub>2</sub>. *Nano Lett.* **14**, 4592–4597 (2014).
- Feng, J., Qian, X., Huang, C.-W. & Li, J. Strain-engineered artificial atom as a broad-spectrum solar energy funnel. *Nat. Photon.* **6**, 866–872 (2012).
- Hwang, H., Kim, H. & Cho, J. MoS<sub>2</sub> nanoplates consisting of disordered graphene-like layers for high rate lithium battery anode materials. *Nano Lett.* **11**, 4826–4830 (2011).
- Lacey, S. D. *et al.* Atomic force microscopy studies on molybdenum disulfide flakes as sodium-ion anodes. *Nano Lett.* **15**, 1018–1024 (2015).
- Hu, L. R., Ren, Y. M., Yang, H. X. & Xu, Q. Fabrication of 3D hierarchical MoS<sub>2</sub>/polyaniline and MoS<sub>2</sub>/C architectures for lithium-ion battery applications. *ACS Appl. Mater. Inter.* **6**, 14644–14652 (2014).
- Kibsgaard, J., Chen, Z., Reinecke, B. N. & Jaramillo, T. F. Engineering the surface structure of MoS<sub>2</sub> to preferentially expose active edge sites for electrocatalysis. *Nat. Mater.* **11**, 963–969 (2012).
- Chou, S. S. *et al.* Understanding catalysis in a multiphase two-dimensional transition metal dichalcogenide. *Nat. Commun.* **6**, 8311 (2015).
- Wang, Y. *et al.* Monolayer PtSe<sub>2</sub>, a new transition-metal-dichalcogenide, grown by direct selenization, shows promise for photocatalysis and valleytronics. *Nano Lett.* **15**, 4013–4018 (2015).
- Sarkar, D. *et al.* MoS<sub>2</sub> field-effect transistor for next-generation label-free biosensors. *ACS Nano* **8**, 3992–4003 (2014).
- Perkins, F. K. *et al.* Chemical vapor sensing with monolayer MoS<sub>2</sub>. *Nano Lett.* **13**, 668–673 (2013).
- Lee, J. *et al.* Two-dimensional layered MoS<sub>2</sub> biosensors enable highly sensitive detection of biomolecules. *Sci. Rep.* **4**, 7352 (2014).
- Shen, J. *et al.* Liquid phase exfoliation of two-dimensional materials by directly probing and matching surface tension components. *Nano Lett.* **15**, 5449–5454 (2015).
- Nicolosi, V., Chhowalla, M., Kanatzidis, M. G., Strano, M. S. & Coleman, J. N. Liquid exfoliation of layered materials. *Science* **340**, 1226419 (2013).
- Haar, S. *et al.* Enhancing the liquid-phase exfoliation of graphene in organic solvents upon addition of *n*-octylbenzene. *Sci. Rep.* **5**, 16684 (2015).
- Du, M., Cui, L., Cao, Y. & Bard, A. J. Mechano-electrochemical catalysis of the effect of elastic strain on a platinum nanofilm for the ORR exerted by a shape memory alloy substrate. *J. Amer. Chem. Soc.* **137**, 7397–7403 (2015).
- Paton, K. R. *et al.* Scalable production of large quantities of defect-free few-layer graphene by shear exfoliation in liquids. *Nat. Mater.* **13**, 624–630 (2014).
- Eda, G. *et al.* Photoluminescence from chemically exfoliated MoS<sub>2</sub>. *Nano Lett.* **11**, 5111–5116 (2011).
- Conley, H. J. *et al.* Bandgap engineering of strained monolayer and bilayer MoS<sub>2</sub>. *Nano Lett.* **13**, 3626–3630 (2013).
- Hui, Y. Y. *et al.* Exceptional tunability of band energy in a compressively strained trilayer MoS<sub>2</sub> sheet. *ACS Nano* **7**, 7126–7131 (2013).
- Rice, C. *et al.* Raman-scattering measurements and first-principles calculations of strain-induced phonon shifts in monolayer MoS<sub>2</sub>. *Phys. Rev. B* **87**, 081307 (2013).
- Lanzillo, N. A. *et al.* Temperature-dependent phonon shifts in monolayer MoS<sub>2</sub>. *Appl. Phys. Lett.* **103**, 093102 (2013).
- MacManus-Driscoll, J. L. Self-assembled heteroepitaxial oxide nanocomposite thin film structures: designing interface-induced functionality in electronic materials. *Adv. Funct. Mater.* **20**, 2035–2045 (2010).
- Stephenson, T., Li, Z., Olsen, B. & Mitlin, D. Lithium ion battery applications of molybdenum disulfide (MoS<sub>2</sub>) nanocomposites. *Energy Environ. Sci.* **7**, 209–231 (2014).
- Chang, K. & Chen, W. L-cysteine-assisted synthesis of layered MoS<sub>2</sub>/graphene composites with excellent electrochemical performances for lithium ion batteries. *ACS Nano* **5**, 4720–4728 (2011).
- Jiang, H. *et al.* 2D monolayer MoS<sub>2</sub>-carbon interoverlapped superstructure: engineering ideal atomic interface for lithium ion storage. *Adv. Mater.* **27**, 3687–3695 (2015).
- Zhu, C., Mu, X., van Aken, P. A., Maier, J. & Yu, Y. Fast Li storage in MoS<sub>2</sub>-graphene-carbon nanotube nanocomposites: advantageous functional integration of 0D, 1D, and 2D nanostructures. *Adv. Energy Mater.* **5**, 4 (2015).
- Zhu, C., Mu, X., van Aken, P. A., Yu, Y. & Maier, J. Single-layered ultrasmall nanoplates of MoS<sub>2</sub> embedded in carbon nanofibers with excellent electrochemical performance for lithium and sodium storage. *Angew. Chem. Int. Ed.* **53**, 2152–2156 (2014).
- Li, W. *et al.* High-performance hollow sulfur nanostructured battery cathode through a scalable, room temperature, one-step, bottom-up approach. *Proc. Natl Acad. Sci. USA* **110**, 7148–7153 (2013).

44. Yeon, J.-T. *et al.* Raman spectroscopic and X-ray diffraction studies of sulfur composite electrodes during discharge and charge. *J. Electrochem. Soc.* **159**, A1308–A1314 (2012).

### Acknowledgements

We thank Nitin Muralidharan and Professor Rizia Bardhan for insightful discussions. This work was supported by the National Science Foundation under CMMI grant #1334269 and Vanderbilt start-up funds. TEM images were obtained from an instrument made possible by NSF grant EPS 1004083. A.P.C. and K.S. are supported by an NSF graduate fellowship under grant # 1445197.

### Author contributions

L.O. and C.L.P. jointly conceived the project and designed the experiments. L.O. and T.H. performed material fabrication with insights from K.S., and L.O. carried out device testing and performance analysis. R.C. performed TEM imaging and analysis, and A.P.C. performed X-ray diffraction measurements and analysis. B.S. performed XPS measurements and analysis. L.O. and C.L.P. wrote the manuscript and all authors participated in discussion and reviewed the manuscript before submission.

### Additional information

**Supplementary Information** accompanies this paper at <http://www.nature.com/naturecommunications>

**Competing financial interests:** The authors declare no competing financial interests.

**Reprints and permission** information is available online at <http://npg.nature.com/reprintsandpermissions/>

**How to cite this article:** Oakes, L. *et al.* Interface strain in vertically stacked two-dimensional heterostructured carbon-MoS<sub>2</sub> nanosheets controls electrochemical reactivity. *Nat. Commun.* **7**:11796 doi: 10.1038/ncomms11796 (2016).



This work is licensed under a Creative Commons Attribution 4.0 International License. The images or other third party material in this article are included in the article's Creative Commons license, unless indicated otherwise in the credit line; if the material is not included under the Creative Commons license, users will need to obtain permission from the license holder to reproduce the material. To view a copy of this license, visit <http://creativecommons.org/licenses/by/4.0/>